

# Reconfigurable Planar Capacitive Coupling in Substrate-Integrated Coaxial-Cavities Filters

Akash Anand, *Student Member, IEEE*, and Xiaoguang Liu, *Member, IEEE*

**Abstract**—This paper expands upon the authors previous work on planar tunable capacitive coupling structures in substrate-integrated cavities using lumped components. We demonstrate both frequency and bandwidth tunable filters with adjustable transmission zeros (TZs). By the appropriate choice of the absolute and relative strength of magnetic and electric coupling coefficients, we demonstrate 1) tunable bandwidth and the ability to maintain either a constant absolute bandwidth or a constant fractional bandwidth; 2) adjustable transmission zero location at a prescribed bandwidth; 3) the ability to switch off the filter with high isolation. Filter design methodologies based on a dispersive coupling structure are presented using lumped circuit models, coupling matrix, and full-wave simulations. With this planar capacitive coupling, it is also convenient to realize cross-coupling in higher order filters to produce additional TZs for rejecting spurious resonances or interferences. Fabricated two-pole filters with one or two TZs and four-pole filters with three or four TZs validate the filter design. A two-pole filter with tunable center frequency and tunable bandwidth along with a four-pole filter with tunable center frequency and tunable TZs are also demonstrated.

**Index Terms**—coaxial cavity resonator, coaxial cavity filter, combline filter, evanescent-mode filter, tunable bandwidth, tunable filters, tunable resonators, constant bandwidth filter

## I. INTRODUCTION

OVER the past decades, metallic cavity resonators have been the dominant choice for highly-selective low-loss filters in RF systems [1]. But with today's diverse technology applications and demands, interest in other filter technologies and topologies is growing, including tunable filters. Various works have shown promising results in some areas of performance but usually at the cost of performance in other parameters. For example, substrate-integrated waveguide (SIW) cavity filters have gained considerable interest in RF/microwave systems for their easy fabrication and low cost compared to traditional air-filled cavities at the expense of lower unloaded quality factor ( $Q_u$ ) due to substrate loss [2], [3]. Nevertheless, SIW filters find a middle ground between low-Q planar and traditional high-Q cavity filters.

To realize compact size evanescent-mode (EVA) filters, cavities are capacitively loaded with a center post, where the bottom end of the center post is shorted while the top end has a small capacitive gap [1], [4], [5]. Magnetic fields are

This paper is an expanded paper from the IEEE Wireless and Microwave Technology Conference (WAMICON) held on June 6, 2014 in Tampa, FL.

A. Anand and X. Liu are with the Department of Electrical and Computer Engineering, University of California at Davis, Davis, CA 95616 USA (e-mail: akaanand@ucdavis.edu; lxgliu@ucdavis.edu).

The authors would like to thank the National Defense Science and Engineering Graduate Program and the University of California, Davis Hellman Fellows Program for supporting this research.

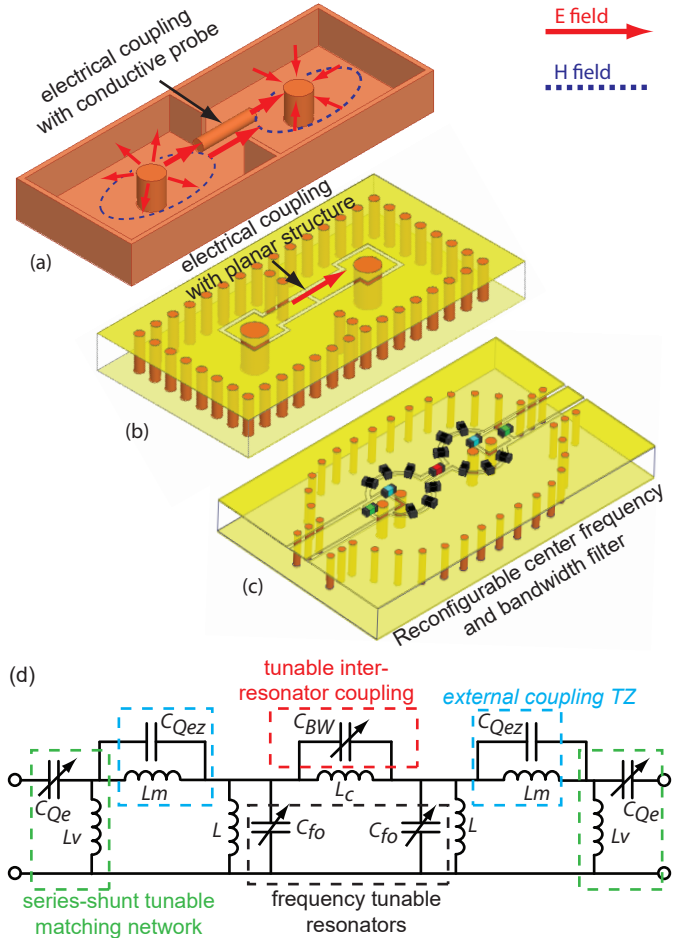


Fig. 1. (a) Coaxial-cavity filter with traditional electric coupling and (b) proposed substrate integrated filter with planar electric coupling. (c) Tunable filter with lumped components and (d) equivalent circuit model for tunable filter.

stronger in the shorted end and electric fields are stronger in the loaded end [6]. Fig. 1(a) shows that EVA cavities magnetically couple through openings in the cavity wall (iris) and electrically couple through a conductive metal probe suspended between the cavity's center posts. Traditionally in such cavities, coupling between resonators is predominantly magnetic (inductive) since it is easier to implement compared to electric (capacitive) coupling probes. For this reason, other methods for electric coupling are presented in [6]–[9]. With appropriate location of iris openings and spacing of the center conductors, works from [6] and [7] realize mixed electric and magnetic coupling without using conductive probes. To make fabrication even simpler, others use planar structures in

SIW filters. For example, Shen et al. use inter-digital slot-line between resonators [8] and Gong et al. use embedded short-ended strip line between two PCB layers to realize electric coupling [9]. Nevertheless, all of these works present fixed coupling structures.

It is desirable to electrically tune the capacitive coupling to realize reconfigurable BW cavity filters. But little work has been done towards this. For example, work from [10] shows an EVA mode topology with surface mount PIN diodes to tune the coupling discretely. The fabrication for this filter requires precise assembly to align the piezo-actuator with the cavity's post and requires multiple PCB layers to integrate the PIN diodes. Work from [11] shows continuously tunable electric coupling with surface mount varactors in SIW filters, but this structure is mostly appropriate for bandstop filters.

It would be convenient to integrate lumped components into SIW cavities with a standard surface mount process to tune the coupling as it is done in planar microstrip or co-planar waveguide (CPW) filters. For example, numerous planar filters with tunable BW have been presented [12]–[20]. To this end, the authors introduced a new substrate-integrated planar capacitive coupling structure for inter-resonator coupling in [21], where a surface mount varactor tunes the coupling. Works from [22]–[24] then use a similar structure in higher order filters to realize both capacitive inter-resonator coupling and capacitive cross-coupling. However, an in depth analysis of this mixed electric and magnetic coupling is needed, in particular, to design for the transmission zero (TZ) that arises due to this dispersive inter-resonator coupling [21].

This paper extends upon the work presented in [21]. While a transmission zero due to dispersive inter-resonator coupling [7], [25], [26] is briefly mentioned in [21], this work presents a more detailed filter design method to place the TZ at a specified location for a prescribed fractional bandwidth (FBW) based on lumped circuit models, coupling matrix, and simulation curves. In addition, the presented external coupling structure adds another TZ above the passband. Surface mount components are easily integrated into the filter to tune the center frequency, BW, and TZs. To validate the filter design, we first fabricate and measure two-pole filters with one or two TZs and four-pole filters with three or four TZs. We then extend these designs to reconfigurable filters. We present a two-pole filter with tunable frequency and tunable BW and a four-pole filter with tunable center frequency and tunable transmission zeros.

## II. COAXIAL-CAVITY RESONATOR

The filter in Fig. 1(b) is based on the coaxial cavity resonator presented in [27]. A coaxial transmission is shorted on the bottom end while a ring gap on the top surface isolates the center conductor from the rest of the cavity's top surface. The ring gap capacitively loads the coaxial cavity. This 3D structure is analogous to planar combline filter where microstrip transmission lines are capacitively loaded. With capacitive loading, the coaxial transmission line is seen as an inductive element and hence resonates like a LC tank [5]. Varactors mounted on the ring gap tune the center frequency  $f_o$

of the resonator [28]–[31]. Works from [27] and [32] present theoretical analysis on this resonator which is summarized below in Eqns. (1)–(6).

The angular resonant frequency  $\omega_o$  is approximated as

$$\omega_o = \frac{1}{\sqrt{LC}} \quad (1)$$

where the loaded capacitance  $C$  is given by

$$C = C_v + C_o \quad (2)$$

in which  $C_v$  is equivalent capacitance of all the frequency tuning varactors  $C_{fo}$  and  $C_o$  is the surface gap capacitance. The inductance  $L$  of the coaxial transmission line (ignoring surface inductance) is given by

$$L = \frac{Z_o}{\omega} \tan \left( \frac{\omega h \sqrt{\epsilon_r}}{c} \right) \quad (3)$$

where  $Z_o$  is the characteristic impedance,  $h$  is the height of the cavity,  $\epsilon_r$  is the dielectric constant, and  $c$  is the speed of light in air. For circular cavities,  $Z_o$  is given in Eqn. (4a) and for square cavities,  $Z_o$  is given in Eqn. (4b),

$$Z_o = \frac{60}{\sqrt{\epsilon_r}} \ln(b/a) \quad (4a)$$

$$Z_o = \frac{60}{\sqrt{\epsilon_r}} \ln \left( 1.079 \frac{s}{a} \right) \quad (4b)$$

where  $a$  is the radius of the inner conductor,  $b$  is the radius of the outer conductor and  $s$  the length of one side of the square cavity's wall.

The  $Q_u$  is approximated as

$$\frac{1}{Q_u} = \frac{1}{Q_c} + \frac{1}{Q_v} \quad (5)$$

where  $Q_v$  is the quality factor of the  $C_{fo}$  varactors and  $Q_c$  is quality factor of just the circular resonator (without  $C_{fo}$ ),

$$Q_c = \frac{\omega_o L}{\frac{R_s}{2\pi} \left( \frac{h}{a} + \frac{h}{b} + 2 \ln(b/a) \right)} \quad (6)$$

in which  $R_s$  is the surface resistance.

## III. DISPERSIVE INTER-RESONATOR COUPLING

Fig. 1(b) shows the proposed filter with electric coupling, where the conductive probe from the traditional filter in Fig. 1(a) is moved to the surface as a planar structure which resembles a CPW transmission line. There is a gap in the middle of this CPW line which separates the two resonators. The traditional filter in Fig. 1(a) and proposed filter Fig. 1(b) both still have the same inter-resonator magnetic coupling, where magnetic fields around the center posts couple to each other through the iris opening in the resonators' adjacent wall. Thus, the presented filter has a mixed electric and magnetic inter-resonator coupling structure.

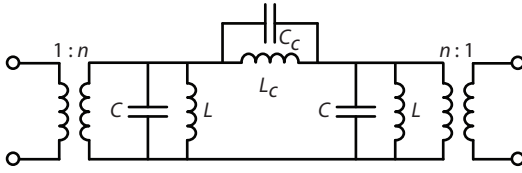


Fig. 2. Lumped circuit model for inter-resonator coupling. The parallel combination of  $L_c$  and  $C_c$  creates a TZ at  $f_{z1} = 1/2\pi\sqrt{L_cC_c}$ .

### A. Filter Design

In order to design filters with this mixed coupling, we first present a lump circuit model that approximates the inter-resonator coupling and aids in visualizing the creation of the TZ. Guidelines are then presented to design filters with a specified TZ location at a prescribed FBW based on the lumped circuit model. Since the 3-D filter structure is complex and coupling depends heavily on filter geometries, more accurate design curves are then presented based on full-wave electromagnetic simulations.

Since the mixed couplings is dispersive [21], it is possible that the magnetic coupling equals the electric coupling at a certain frequency and a TZ occurs. Previous works from [7]–[9], [25], [26], [33] report this TZ in 3-D structures, which is easier to visualize with the lumped circuit model in Fig. 2. Inductance  $L$  and capacitance  $C$  model the bandpass resonators while  $L_c$  and  $C_c$  represent the inductive and capacitive coupling [4]. The parallel combination of  $L_c$  and  $C_c$  creates a TZ ( $TZ_1$ ) at

$$f_{z1} = \frac{1}{2\pi\sqrt{L_cC_c}}. \quad (7)$$

Consider the case when the electric coupling and magnetic coupling are equal at the center frequency, then  $TZ_1$  occurs at center frequency or  $f_{z1} = f_o$ . If the electric coupling increases or the magnetic coupling decreases, then  $TZ_1$  moves below the passband ( $C_c$  and  $L_c$  both increase). Conversely, if the magnetic coupling increases and the electric coupling decreases, then  $TZ_1$  moves above the passband ( $C_c$  and  $L_c$  both decrease). Once the side of the  $TZ_1$  is determined (above or below passband), then the exact location of the  $TZ_1$  can be designed by either increasing or decreasing both the electric and magnetic coupling together in order to maintain a constant FBW. Consider the various filter designs with constant 6% 3-dB FBW but different  $TZ_1$  locations in Table I based on the lumped circuit model in Fig. 2. For filters with  $TZ_1$  below the passband,  $L_c$  decreases from 47.5 nH to 6.44 nH and  $C_c$  increases from 0.1 pF to 0.5 pF to move  $TZ_1$  higher in frequency closer to the passband. For filters with  $TZ_1$  above the passband,  $C_c$  increases from 0.1 pF to 0.5 pF and  $L_c$  decreases from 19.6 nH to 5.01 nH to move  $TZ_1$  lower in frequency closer to the passband. Fig. 3 shows  $S_{21}$  for selected examples from the table. Based on the above discussion and Table I, we can summarize the following for filters designed at  $f_o$  with a fixed FBW:

- (a) When electric coupling is dominant,  $TZ_1$  is below the passband.
- (b) When magnetic coupling is dominant,  $TZ_1$  is above the passband.

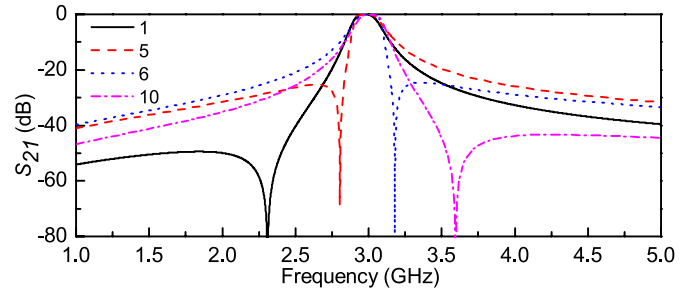


Fig. 3. Selected examples from Table I with filters designed with 6% FBW but different  $TZ_1$  locations based on lumped circuit model from Fig. 2.

- (c) Below the passband,  $TZ_1$  moves to higher frequency (closer to the passband) as the magnitude of both electric and magnetic coupling increases.
- (d) Above the passband,  $TZ_1$  moves to lower frequency (closer to the passband) as the magnitude of both electric and magnetic coupling increases.

TABLE I  
FILTERS DESIGNED WITH 6% 3-DB FBW AT  $f_o = 3$  GHz BUT WITH DIFFERENT  $TZ_1$  LOCATIONS BASED ON LUMPED CIRCUIT MODEL FROM FIG. 2

filter	$TZ_1$ (GHz)	$n$	$L$ (nH)	$C$ (pF)	$C_c$ (pF)	$L_c$ (nH)
$TZ_1$ below the passband (strongly electric coupling)						
1	2.31	5	3.2	0.85	0.1	47.5
2	2.64	5	3.2	0.85	0.2	18.2
3	2.72	5	3.2	0.85	0.3	11.4
4	2.77	5	3.2	0.86	0.4	8.23
5	2.81	5	3.2	0.86	0.5	6.44
$TZ_1$ above the passband (strongly magnetic coupling)						
6	3.18	5	3.2	0.91	0.5	5.01
7	3.21	5	3.2	0.91	0.4	6.16
8	3.26	5	3.2	0.91	0.3	7.97
9	3.34	5	3.2	0.91	0.2	11.4
10	3.60	5	3.2	0.91	0.1	19.6

The inter-resonator electric and magnetic couplings are defined as  $k_E$  and  $k_M$ . The total inter-resonator coupling  $k$  is then the sum of  $k_E$  and  $k_M$  [4],

$$k = \frac{k_M + k_E}{1 + k_M k_E} \approx k_M + k_E \quad (8)$$

for narrow band filters and  $k$  can be extracted from

$$k = \pm \frac{f_1^2 - f_2^2}{f_1^2 + f_2^2} \quad (9)$$

where  $f_1$  and  $f_2$  are the eigen frequencies of the coupled resonators. Since the signs of magnetic (+) and electric (−) coupling are opposite [21],  $k$  can be either positive, negative, or zero.

According to [34], the required values for  $k$  and external coupling  $Q_e$  for a particular filter design is

$$k_{i,i+1} = \frac{FBW}{\sqrt{g_i g_{i+1}}} \text{ for } i = 1 \text{ to } (n-1) \quad (10)$$

and

$$Q_{e1} = \frac{g_0 g_1}{FBW} \text{ and } Q_{en} = \frac{g_n g_{n+1}}{FBW} \quad (11)$$

where  $n$  is the order of the filter and the  $g$  values are given in any standard filter design reference such as [1], [4], [34].

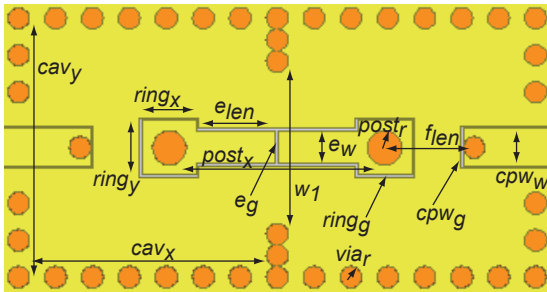


Fig. 4. Two resonators with mixed electric and magnetic inter-resonator coupling and labeled dimensions.

Fig. 4 shows two resonators with inter-resonator coupling designed around 2.7 GHz with dimensions listed in Table II, where  $h$  is the substrate height and  $\epsilon_r$  is the substrate dielectric constant. Fig. 5(a) shows the HFSS simulated  $k$  versus  $e_w$  (width of the electric coupling CPW) at various magnetic wall openings  $w_1$ . The electric coupling becomes stronger (more negative) as  $e_w$  increases. The magnetic coupling increases as  $w_1$  or the iris opening becomes larger. For a prescribed FBW,  $k$  maps to  $w_1$  and  $e_w$  in Fig. 5(a).

In order to externally couple to the filter, CPW transmission lines are used as the input/output feeds which extend inside the cavity where a via shorts them to the bottom. Current flowing through the CPW shorting via creates magnetic fields that couples with the magnetic fields of the center post. A similar feed structure is analyzed in more details in [35]. Fig. 5(b) shows  $Q_e$  versus  $f_{len}$ , where  $f_{len}$  is the distance between center post and the CPW shorting via shown in Fig. 4. For a prescribed FBW,  $Q_e$  maps to  $f_{len}$  in Fig. 5(b).

TABLE II  
VALUES FOR RESONATORS WITH MIXED INTER-RESONATOR COUPLING  
LABELED IN FIG 4.

parameter	value	parameter	value
$cav_x$	22 mm	$cpw_w$	3.5 mm
$cav_y$	22 mm	$cpw_g$	0.18 mm
$h$	6.35 mm	$f_{len}$	10 mm
$ring_x$	5.0 mm	$e_{len}$	14.51 mm
$ring_y$	5.0 mm	$e_g$	0.26 mm
$ring_g$	0.26 mm	$e_w$	1.0 mm
$post_r$	1.59 mm	$w_1$	20.0 mm
$post_x$	20.0 mm	$\epsilon_r$	2.2
$via_r$	1.01 mm		

A filter with prescribed FBW and flexible  $TZ_1$  location can be designed based on the guidelines from the lumped circuit model. For example, when  $TZ_1$  is above the passband, increasing  $e_w$  moves  $TZ_1$  lower in frequency. Conversely, when  $TZ_1$  is below the passband, increasing  $w_1$  moves  $TZ_1$  higher in frequency. For a given  $e_w$  or  $w_1$ , the corresponding  $w_1$  and  $e_w$  are chosen according to Fig. 5(a) to keep a constant  $|k|$ . Note that  $k$  can take negative values at larger  $e_w$ . When  $k$  is negative, electric coupling is stronger and  $TZ_1$  is below the passband, while when  $k$  is positive, magnetic coupling is stronger and  $TZ_1$  is above the passband.

Alternatively coupling matrix theory can be used to design the filters. Works from [36] and [37] provide design guidelines to generate the coupling matrix at a fixed frequency. But

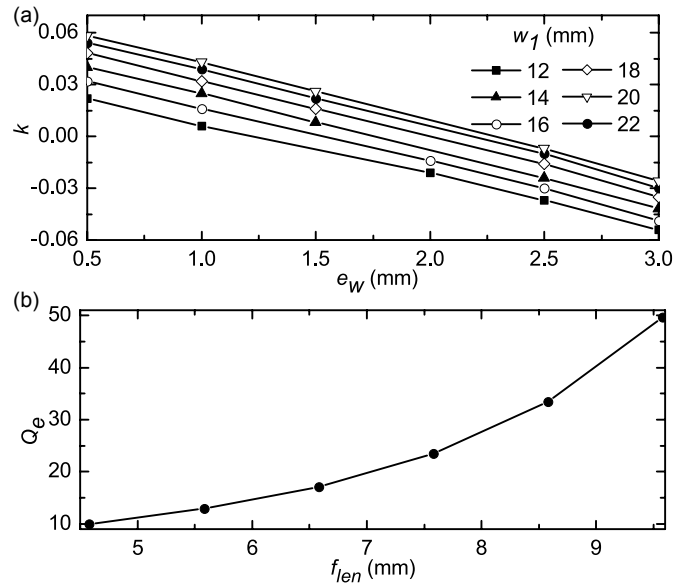


Fig. 5. Simulated (a)  $k$  versus  $e_w$  at various  $w_1$  values and (b)  $Q_e$  versus  $f_{len}$  around 2.7 GHz.

dispersive coupling filters need frequency depended coupling matrix to accurately model the frequency response. These frequency dependent inter-resonator coupling parameters can be simulated and extracted from HFSS. The steps below give an iterative design procedure to design filters with frequency depended coupling matrix.

- 1) Generate the coupling matrix for a filter with desired specifications without dispersive coupling based on standard coupling matrix design in [36] and [37].
- 2) Generate a series of frequency dependent inter-resonator coupling  $k(\omega)$  curves for different FBW using a full-wave electromagnetic solver (Fig. 5(a)).
- 3) Extract the inter-resonator coupling  $m(\omega)$  values from simulated  $k(\omega)$  curves.
- 4) Re-optimize coupling matrix values other than the dispersive inter-resonator coupling  $m(\omega)$  using numerical simulations (s-parameter).
- 5) Based on the guidelines earlier and using the design curve from step 2, increase or decrease the both electric and magnetic coupling to move the  $TZ_1$  while keeping  $k$  constant.
- 6) Repeat steps 3 and 5 to get the desired FBW and  $TZ$  location.

Examples of such matrix design is presented in Section III-B and section III-C along with simulated and measured results.

### B. Two-Pole Filter Example

To illustrate examples of dispersive coupling matrix, two two-pole filters are designed based on guidelines from Section III-A: filter  $M_1$  has 6.3% 3-dB FBW and filter  $M_2$  has 8.0% 3-dB FBW around 2.75 GHz. Fig. 6(c) shows the simulated  $k$  versus frequency for the two filters, where a second order polynomial  $k_{12}(\omega)$  fits the simulation data. A TZ ( $TZ_1$ ) occurs when  $k_{12} = 0$ . For  $M_1$ ,  $k_{12} = 0$  is below the passband around 2.1 GHz and for  $M_2$ ,  $k_{12} = 0$

is above the passband around 3.6 GHz. Eqns. (12) and (13) show the coupling matrix with frequency dependent inter-resonator coupling  $m_{12}(\omega)$  extracted from  $k_{12}(\omega)$ . Fig. 6(a) and (b) show the fabricated filters with SMA connectors. The dimensions are the same as those listed in Table II, except for  $M_1$ ,  $f_{len} = 8.28$  mm,  $e_w = 3$  mm and  $w_1 = 14$  mm, and for  $M_2$ ,  $f_{len} = 8.08$  mm,  $e_w = 1$  mm and  $w_1 = 22$  mm. Fig. 6(d) and (e) plot the coupling matrix along with simulated and measured data. Simulated and measured insertion loss in the passband is 0.58 dB and 0.45 dB for  $M_1$  and 0.41 dB and 0.38 dB for  $M_2$ .

$$M_1(\omega) = \begin{bmatrix} 0 & 0.698 & 0 & 0 \\ 0.698 & 0 & m_{12}(\omega) & 0 \\ 0 & m_{12}(\omega) & 0 & 0.698 \\ 0 & 0 & 0.698 & 0 \end{bmatrix} \quad (12)$$

$$\begin{aligned} m_{12}(\omega) &= k_{12}(\omega) \times FBW \\ &= -0.007 \left( \frac{\omega}{10^9} \right)^2 + 0.070 \frac{\omega}{10^9} + 0.354 \end{aligned}$$

$$M_2(\omega) = \begin{bmatrix} 0 & 0.774 & 0 & 0 \\ 0.774 & 0 & m_{12}(\omega) & 0 \\ 0 & m_{12}(\omega) & 0 & 0.774 \\ 0 & 0 & 0.774 & 0 \end{bmatrix} \quad (13)$$

$$\begin{aligned} m_{12}(\omega) &= k_{12}(\omega) \times FBW \\ &= -0.005 \left( \frac{\omega}{10^9} \right)^2 + 0.1150 \frac{\omega}{10^9} + 0.0325 \end{aligned}$$

### C. Higher Order Filters with Cross-Coupling

In addition to designing filters with dispersive coupling in adjacent resonators, we can use the presented structure in cross-coupled resonators to design higher order filters with additional TZs [23], [24]. For example, Fig. 7 shows the coupling schematic for four-pole cross-coupled filters. Filters in Fig. 7(a) and (b) have all inductive coupling between resonators except for the capacitive coupling between resonators 1 and 4 in Fig. 7(a) and between resonators 2 and 3 in Fig. 7(b). In both filters, the main line path (1, 2, 3, and 4) and cross coupling path (1 and 4) are out of phase and add destructively to create a pair of TZs [38]. This is verified with coupling matrix given in Eqn. (14) and plotted in Fig. 8. Both filters have the same coupling matrix except for the coupling sign between resonators 1 and 4 and between resonators 2 and 3, which is positive (+) when the coupling is inductive and negative (-) when the coupling is capacitive.

$$M_3 = \begin{bmatrix} 0 & 1.02 & 0 & 0 & 0 & 0 \\ 1.02 & 0 & 0.856 & 0 & \mp 0.220 & 0 \\ 0 & 0.856 & 0 & \pm 0.786 & 0 & 0 \\ 0 & 0 & \pm 0.786 & 0 & 0.856 & 0 \\ 0 & \mp 0.220 & 0 & 0.856 & 0 & 1.02 \\ 0 & 0 & 0 & 0 & 1.02 & 0 \end{bmatrix} \quad (14)$$

Mixed cross-coupling between resonators 1 and 4 generates a third TZ compared to purely inductive or capacitive [6],

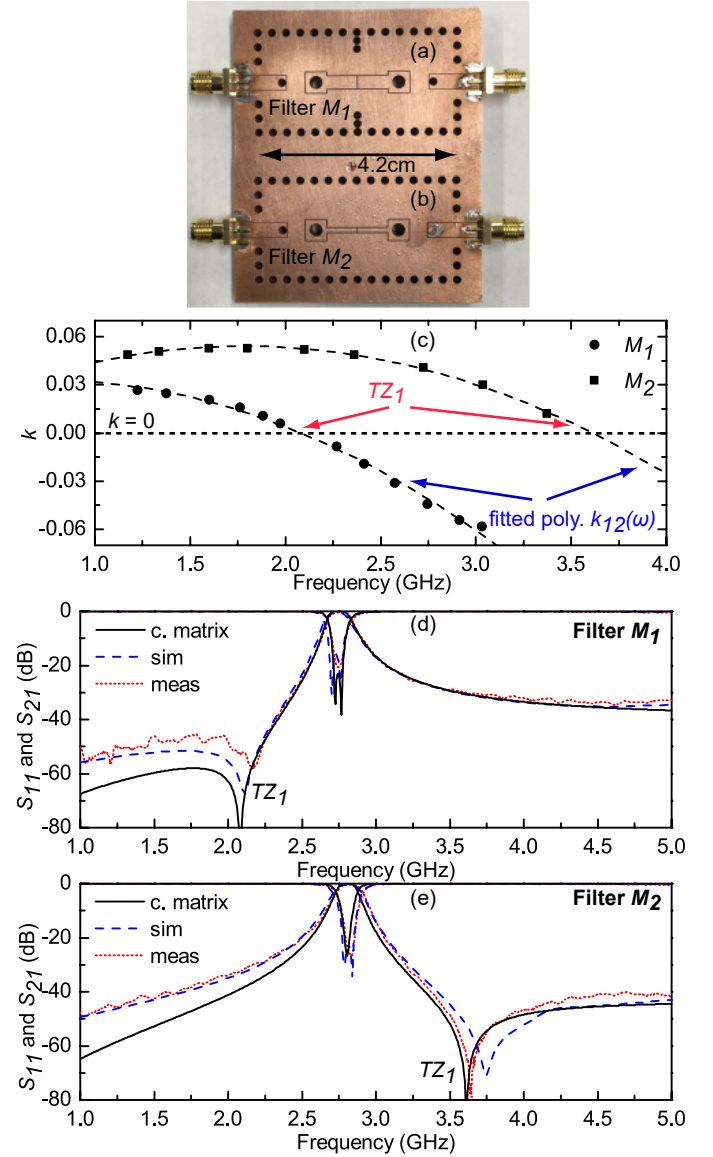


Fig. 6. Fabricated two-pole filters (a)  $M_1$  and (b)  $M_2$  and (c) HFSS simulated dispersive inter-resonator  $k$  for designed filters. Plots of measured, simulated and coupling matrix in (d) Eqn. (12) and (e) Eqn. (13).

[39]. Fig. 7(c) and (d) show the schematic for mixed cross-coupling between resonator 1 and 4. This work qualitatively discusses the presence of all three TZs while additional analysis is presented in [6]. In the passband, the magnitude of main line path with resonators 1, 2, 3, and 4 (four-pole filter) is dominant compared to magnitude of the cross-coupled resonators 1 and 4 (two-pole filter). As  $\omega$  moves away from the passband, the magnitude of the four-pole filter (main line path) falls faster than the magnitude of the two-pole filter (cross-coupling path). A pair of real frequency TZ ( $TZ_2$  and  $TZ_3$ ) results when the magnitude of the main line coupling and the magnitude of the cross-coupling are the same at frequencies  $f_{z2}$  and  $f_{z3}$ . Beyond  $f_{z2}$  and  $f_{z3}$ , the two-pole filter (cross-coupling path) is dominant and  $TZ_1$  appears at  $f_{z1}$  due to the inter-resonator coupling (same TZ from section III-A).  $TZ_1$  can be placed anywhere below  $TZ_2$  or above  $TZ_3$ .

$$M_4(\omega) = \begin{bmatrix} 0 & 1.164 & 0 & 0 & 0 & 0 \\ 1.164 & 0 & 0.957 & 0 & m_{14}(\omega) & 0 \\ 0 & 0.957 & 0 & 0.851 & 0 & 0 \\ 0 & 0 & 0.851 & 0 & 0.957 & 0 \\ 0 & m_{14}(\omega) & 0 & 0.957 & 0 & 1.164 \\ 0 & 0 & 0 & 0 & 1.164 & 0 \end{bmatrix} \quad m_{14}(\omega) = -0.054 \frac{\omega}{10^9} + 0.623 \quad (15)$$

$$M_5(\omega) = \begin{bmatrix} 0 & 1.114 & 0 & 0 & 0 & 0 \\ 1.114 & 0 & 0.957 & 0 & m_{14}(\omega) & 0 \\ 0 & 0.957 & 0 & -0.843 & 0 & 0 \\ 0 & 0 & -0.843 & 0 & 0.957 & 0 \\ 0 & m_{14}(\omega) & 0 & 0.957 & 0 & 1.114 \\ 0 & 0 & 0 & 0 & 1.114 & 0 \end{bmatrix} \quad m_{14}(\omega) = -0.060 \frac{\omega}{10^9} + 1.1843 \quad (16)$$

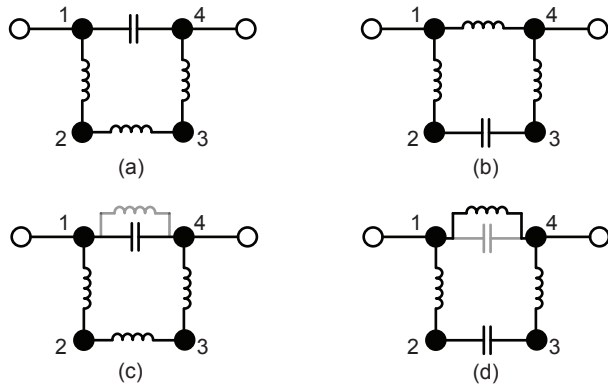


Fig. 7. Coupling schematic for four-pole cross-coupled filters with (a) capacitive cross coupling, (b) inductive cross-coupling, (c) stronger capacitive with weaker inductive cross-coupling and (d) stronger inductive with weaker capacitive cross-coupling.

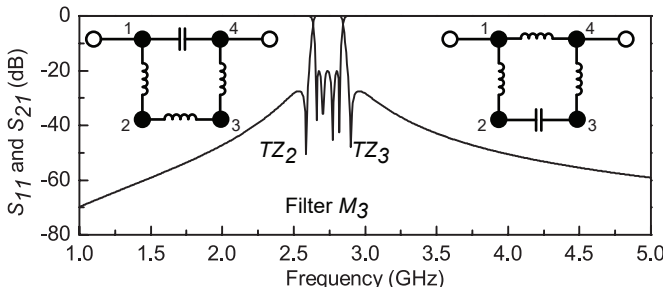


Fig. 8. Both capacitive and inductive cross-coupling from Fig. 7(a) and (b) result in two TZs, one on each side of the passband.

The design procedure for the mixed cross-coupling is the same as that in section III-A, where the magnitude of cross-coupling from the coupling matrix maps to extracted coupling curves from simulation. Eqns. (15) and (16) gives the coupling matrix for two designed filters,  $M_4$  and  $M_5$ , where frequency dependent  $m_{14}(\omega)$  is extracted from HFSS simulation, similar to  $m_{12}(\omega)$  in Eqns. (12) and (13). When mixed cross-coupling is strongly electric,  $TZ_1$  will be below the passband and when the mixed cross-coupling is strongly magnetic,  $TZ_1$  will be above the passband (analogous to Fig. 6(d) and (e)). Fig. 9(a) and Fig. 9(b) show the fabricated filter along with the filter dimensions and SMA connectors. All other dimensions of

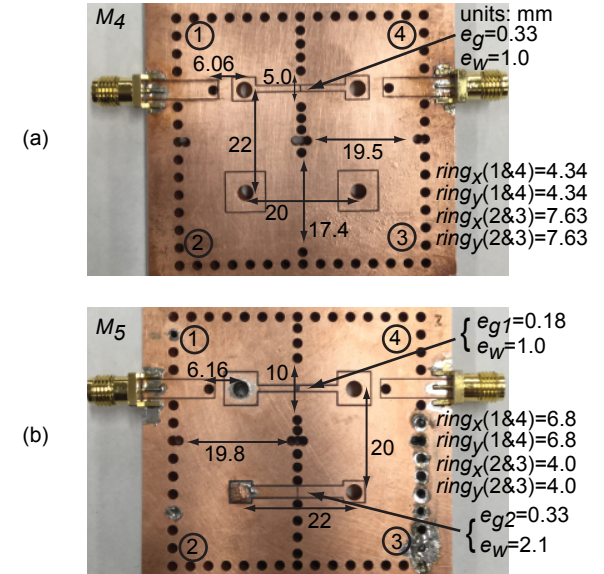


Fig. 9. Fabricated four-pole filter (a)  $M_4$  and (b)  $M_5$  with mixed electric and magnetic coupling.

the filter are same as those labeled in Fig. 4 and listed in Table II. Fig. 10(a) and Fig. 10(b) plot the coupling matrix along with simulated and measured data. The figure also labels the location of  $TZ_1$ ,  $TZ_2$ , and  $TZ_3$ . Simulation shows  $M_4$  has 8.6% FBW and 0.45 dB insertion loss at 2.7 GHz while measurement shows 9.3% FBW and 0.43 dB insertion loss. Simulation shows  $M_5$  has 8.1% FBW and 0.46 dB insertion loss at 2.6 GHz while measurement shows 7.6% FBW and 0.90 dB insertion loss. Incomplete plating of some of the vias degraded insertion loss in  $M_5$  compared to simulation.

#### IV. EXTERNAL COUPLING TZ

Fig. 11(a) shows a modified lumped circuit model from section III-A, where mutual inductance between  $L'_v$  models the external coupling. Another capacitor  $C_{Qez}$  is added in parallel with the mutual inductance. If the mutual inductance is modeled with an equivalent  $\pi$ -network [4], then Fig. 11(a) can be represented as Fig. 11(b), where  $L'_v$  and  $L_m$  are absorbed into  $L$  and  $L_v$ . The series parallel combination of  $L_m$  and

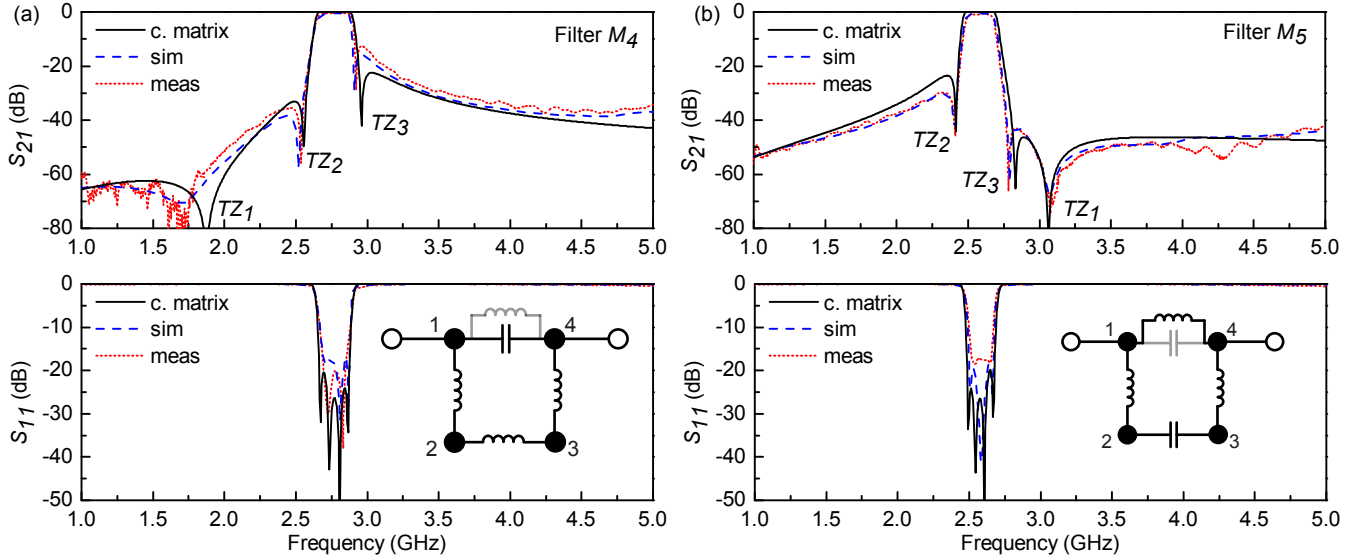


Fig. 10. Plots of measured, simulated, and coupling matrix in (a) Eqn. (15) and (b) Eqn. (16). Compared to Fig. 8, a third notch (TZ<sub>1</sub>) is created (a) below the passband for stronger electric coupling ( $M_4$ ) and (b) above the passband for stronger magnetic coupling ( $M_5$ ).

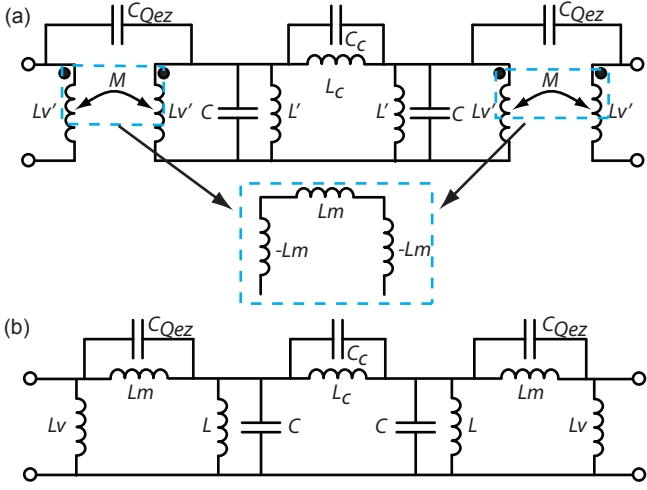


Fig. 11. (a) Lumped circuit model for two-pole filter where mutual inductance models the external coupling. The mutual inductance are modeled with  $\pi$ -networks and (b) shunt  $L_m$  inductance are absorbed into  $L$  and  $L_v$ . The parallel combination of  $L_m$  and  $C_{Qez}$  creates TZs at  $\omega_m = 1/\sqrt{L_m C_{Qez}}$

$C_{Qez}$  creates another pair of TZs (TZ<sub>4</sub>) located at

$$f_{z4} = \frac{1}{2\pi\sqrt{L_m C_{Qez}}}. \quad (17)$$

Fig. 12(a) shows the first method to realize  $C_{Qez}$ , where part of the CPW feed line extends further into the cavity and overlaps with the square ring gap. Some of the input/output energy flows directly into the resonator through this overlap capacitance ( $C_{Qez}$ ) while some energy couples in parallel through the mutual inductance between the center post and CPW shorting post. Measured and simulated results in Fig. 12(b) shows a two-pole filter with TZ<sub>4</sub> above the passband and TZ<sub>1</sub> below the passband. Simulation shows 5.5% FBW and 0.86 dB insertion loss at 2.8 GHz while measurement shows 5.0% FBW and 0.64 dB insertion loss.

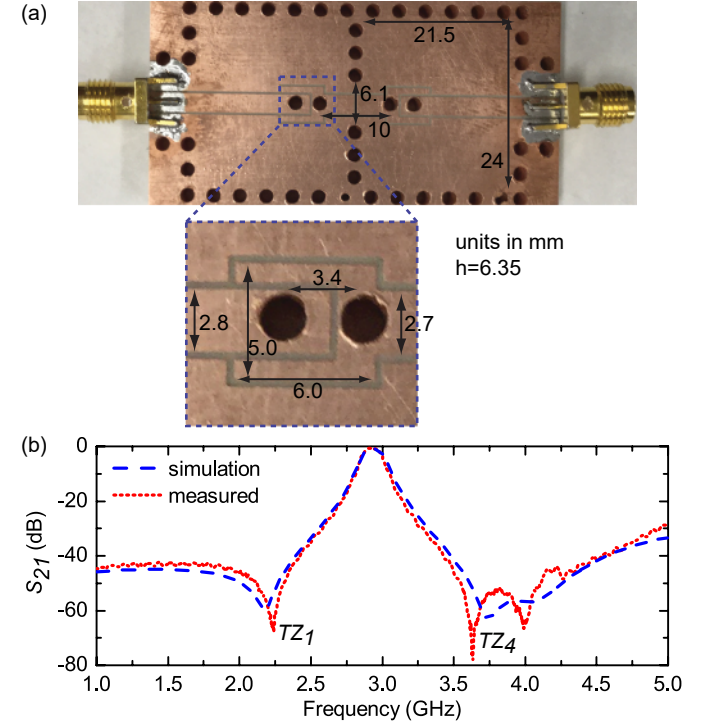


Fig. 12. (a) Fabricated two-pole filter with two zeros where CPW feed line extends further into the cavity and overlaps with the square ring gap, creating some overlap capacitance  $C_{Qez}$  and (b) measured and simulated s-parameter.

The filter is fabricated on a 6.35 mm Rogers TMM3 substrate with dielectric loss tangent of 0.002.

The second method to realize  $C_{Qez}$  is to use a lumped capacitor. First the filter is designed according to section III and then  $C_{Qez}$  is included and the filter is re-optimized. For example, the four-pole filter  $M_4$  from Fig. 9(a) and Eqn. (15) is redesigned to include TZ<sub>4</sub>. Fig. 13(a) shows the fabricated filter with a close-up view of the surface mount

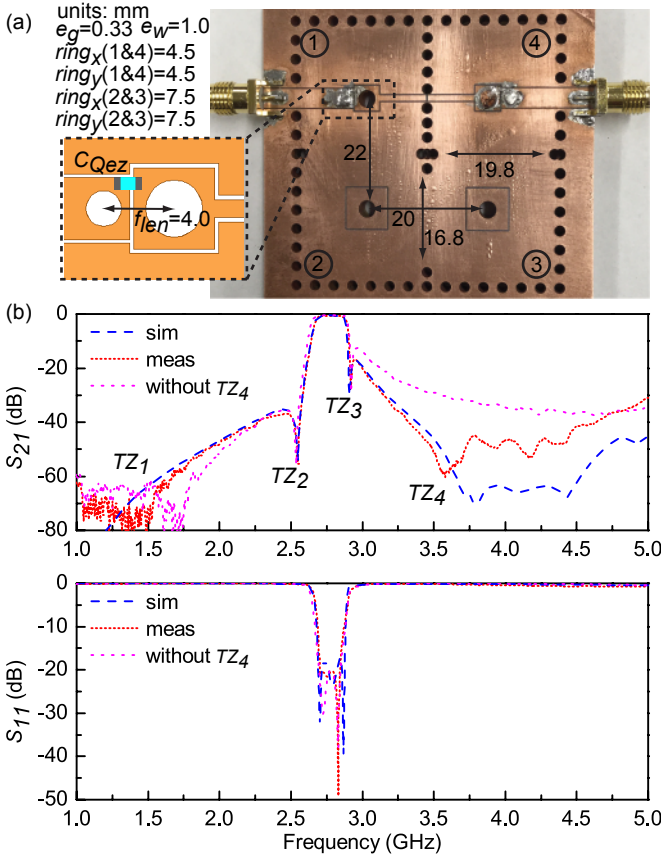


Fig. 13. (a) Fabricated four-pole filter from Fig. 9(a) redesigned to include  $C_{Qez}$  and  $TZ_4$ . (b) Measurement and simulation shows improvement in upper stop band rejection with  $TZ_4$ .

$C_{Qez}$  capacitor. The CPW feed line extends towards the cavity but doesn't overlap with the ring gap and a lumped capacitor instead couples energy parallel to the mutual inductance. Compared to the first method with overlapping capacitance, this method requires less re-optimization to the initial design before  $C_{Qez}$  is added. Mainly, the external coupling parameter  $f_{len}$  needs to be redesigned after adding  $C_{Qez}$ . Fig. 13(a) shows the modified dimensions. The upper passband rejection improves when  $TZ_4$  is included in Fig. 13(b) compared to the same filter without  $TZ_4$ . Simulation shows 7.8% FBW and 0.59 dB insertion loss at 2.7 GHz while measurement shows 8.2% FBW and 0.64 dB insertion loss.

## V. RECONFIGURABLE FILTER

### A. Tunable BW Filter Design

Fig. 1 and Fig. 14 show that the proposed filter is easily integrated with lumped elements to realize a reconfigurable filter. Fig. 1(d) shows the equivalent lumped circuit model for the reconfigurable filter. Varactors  $C_{fo}$  tunes the center frequency, varactor  $C_{BW}$  tunes the BW, varactor  $C_{Qe}$  tunes the external coupling, and capacitors  $C_{Qez}$  produces  $TZ_4$ .

Work from [21] shows that  $Q_u$  up to 200 at 1 GHz can be achieved for frequency-tunable filters while using only  $C_{fo}$  varactors. Adding  $C_{BW}$  in the inter-resonator coupling path degrades  $Q_u$ . To minimize this loss and still achieve BW

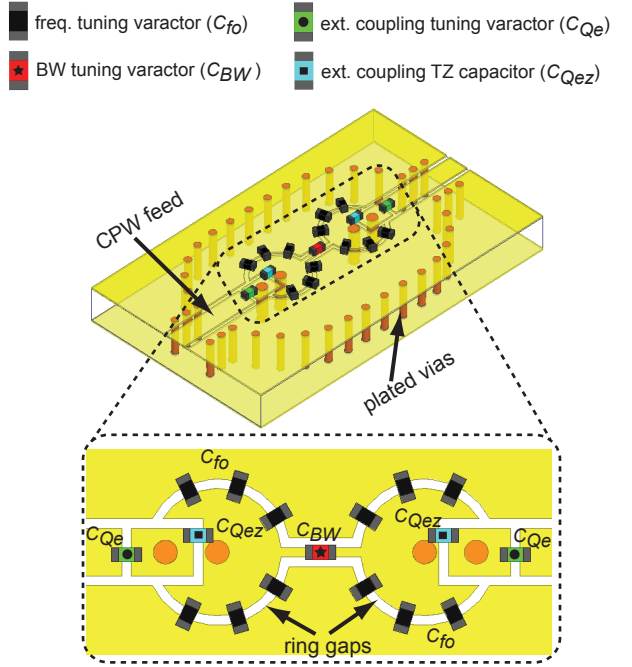


Fig. 14. Tunable two-pole filter and close up of top surface showing the various integrated lumped components.

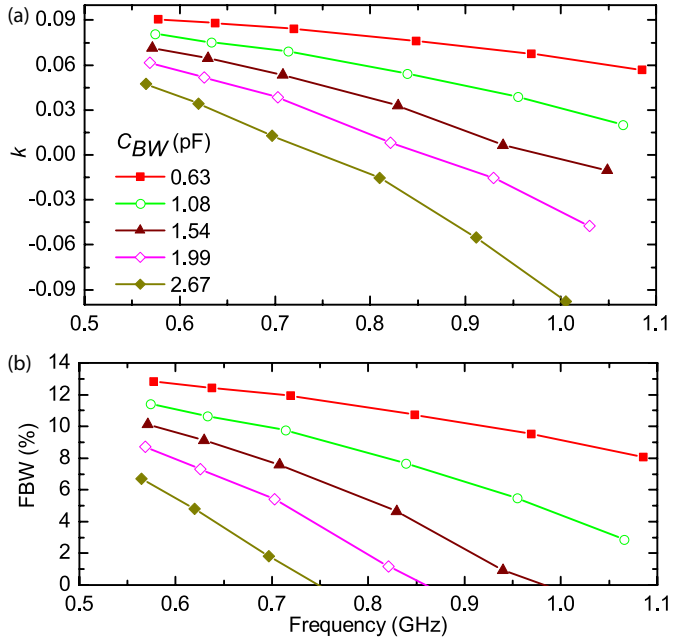


Fig. 15. HFSS simulation for (a)  $k$  versus frequency and (b) FBW solved from Eqn. (10) for a two-pole butterworth filter.

tuning,  $k_M$  is designed to be the dominant inter-resonator coupling path so that most of the electromagnetic energy flows through the magnetic fields instead of the lossy varactors. From the design guidelines in section III-A, a strongly magnetic coupled filter is designed. Fig. 15(a) shows  $k$  versus center frequency for various  $C_{BW}$ . Fig. 15(b) shows the range of FBW solved from Eqn. (10) for a butterworth filter design. Since it is desired that  $k_M$  is dominant, only the

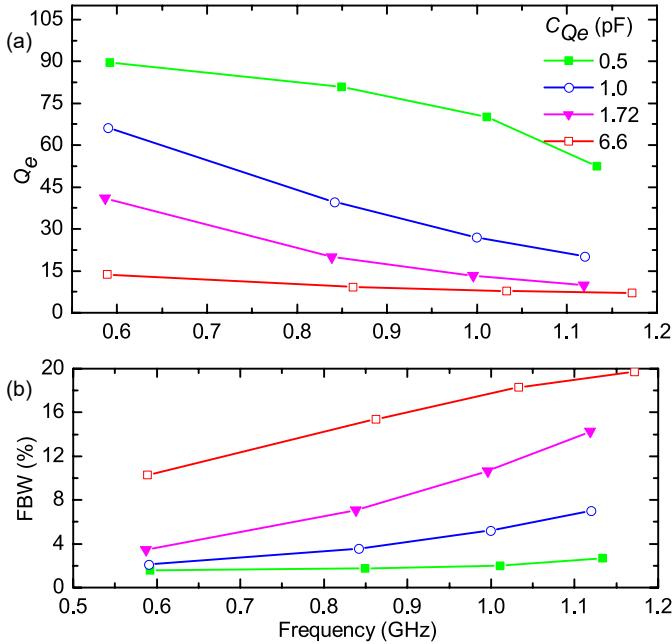


Fig. 16. HFSS simulation for (a)  $Q_e$  versus frequency and (b) FBW solved from Eqn. (11) for a two-pole butterworth filter.

FBW corresponding to the positive values of  $k$  are plotted. Theoretically, this two-pole filter can achieve a FBW of 0–8% around 1.1 GHz and 7–13% FBW around 0.55 GHz, if not limited by  $Q_e$ . The range of FBW at all frequencies is bounded by  $C_{BW} = 0.63$  pF and  $C_{BW} = 2.67$  pF curves.

Fig. 14 shows varactors ( $C_{Qe}$ ) mounted over slits created in the CPW line. The lumped circuit model in Fig. 1(d) shows that  $C_{Qe}$  and  $L_v$  act as a series-shunt matching network. Thus, tuning  $C_{Qe}$  varies the input impedance and tunes  $Q_e$ . Fig. 16(a) shows the HFSS simulation of  $Q_e$  versus frequency as  $C_{Qe}$  is tuned from 0.5 pF to 6.6 pF. The value of  $Q_e$  ranges from 15 to 20 around 0.55 GHz and 7 to 52 around 1.1 GHz. Since  $Q_e$  is known, FBW is extracted from Eqn. (11) and plotted in Fig. 16(b). This gives the range of FBW of the filter, if not limited by  $k$ .

The tuning range for FBW presented in Fig. 15 and Fig. 16 were based on  $k$  and  $Q_e$  independently. The actual tuning range of the filter is given when the effects of both  $k$  and  $Q_e$  is considered together. Thus the extreme values of  $C_{BW} = 0.63$  pF and  $C_{BW} = 2.67$  pF along with the extreme values of  $C_{Qe} = 0.5$  pF and  $C_{Qe} = 6.6$  pF are plotted together in Fig. 17. The tuning range of the filter is bounded (shaded region) by the four curves.

The HFSS simulation in Fig. 18 shows BW tuning of the filter around 1.1 GHz without including  $C_{Qez}$  capacitor. Initially at  $C_{BW} = 0.01$  pF, BW is 170 MHz, and  $TZ_1$  is not observed up to 2 GHz. At  $C_{BW} = 0.63$  pF, BW is 95 MHz and  $TZ_1$  appears at 1.38 GHz. BW decreases further as  $C_{BW}$  increases and  $TZ_1$  moves closer to the passband. At  $C_{BW} = 1.44$  pF,  $k_E \approx k_M$  at the center frequency and  $TZ_1$  is at  $f_o$ : a zero BW filter or the off state of the filter. Fig. 19 shows the simulation result when  $C_{Qez}$  is added to realize  $TZ_4$ . In this case,  $C_{BW}$  is kept at 0.63 pF. Increasing

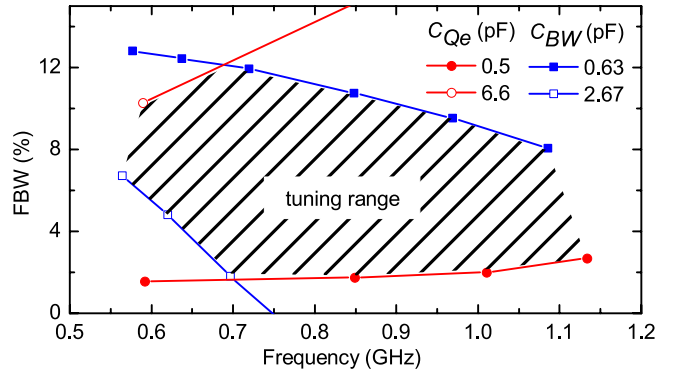


Fig. 17. The shaded region shows the FBW tuning range for the filter as the center frequency tunes from 0.55 GHz to 1.1 GHz.

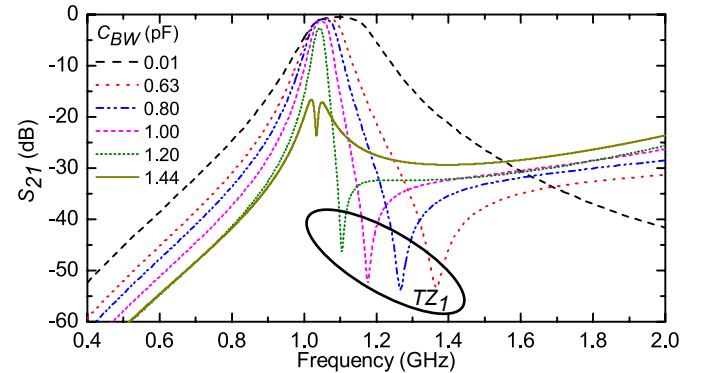


Fig. 18. Simulated tunable BW filter from Fig. 14 without  $C_{Qez}$ . Increasing  $C_{BW}$  decreases BW and tunes  $TZ_1$  closer to the passband.

$C_{Qez}$  moves  $TZ_4$  closer to the passband. Increasing  $C_{Qez}$  also decreases the BW and location of  $TZ_1$  slightly. The dimensions of the simulated filter is given in section V-B.

### B. Tunable BW Filter Validation

The reconfigurable filter from section V-A is fabricated on a Rogers TMM3 board with 5 mm thickness and 0.002 loss tangent. The filter is modified to a double ring structure with additional gaps created on the top surface to mount all the varactors back-to-back. The back-to-back placement of varactors conveniently isolates a dc bias point and improves linearity [40]. Following the guidelines given in [2], vias are drilled in the substrate and plated with copper to form the cavities. The center posts and CPW shorting posts are also created with copper plated vias. The modified filter design is shown in Fig. 20(a) and the fabricated filter with SMA connectors is shown in Figs. 20(b) and (c). Figs. 20(d) and (e) show the dimensions of the board and traces on the top surface. Table. III lists the details of the lumped components used. Additionally, 1-MΩ resistors are used in the dc bias line to reduce RF loss.

The fabricated filter is first measured without the  $C_{Qez}$  capacitor. In Fig. 21(a),  $TZ_1$  is initially at 1.5 GHz but moves closer to the passband as  $C_{BW}$  increases. The BW decreases from 100 MHz to 20 MHz as  $C_{BW}$  increases. Both of these observations are consistent with previous simulation

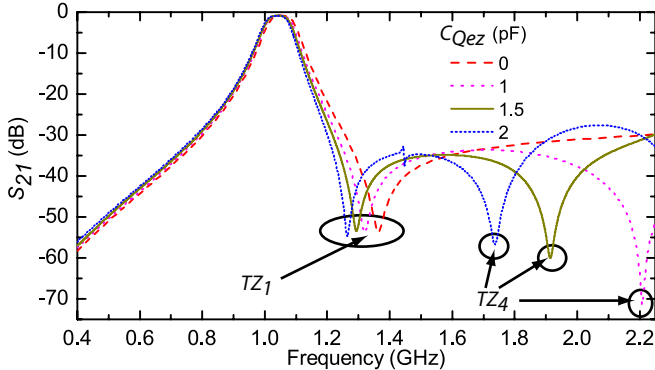


Fig. 19. Tunable filter from Fig. 18 with  $C_{BW} = 0.63$  pF shows  $TZ_4$  changes significantly with  $C_{Qez}$ . Small change in BW and  $TZ_1$  is also observed.

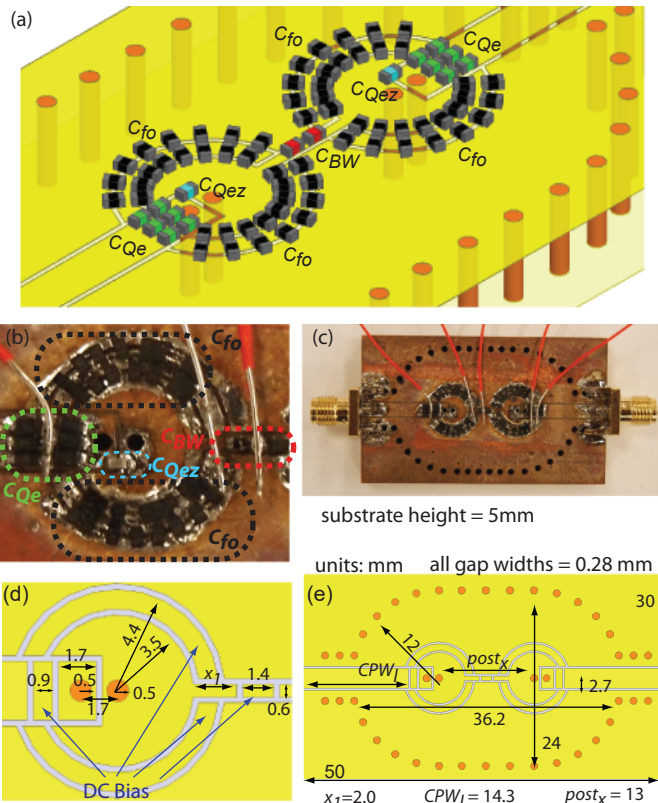


Fig. 20. (a) Designed filter with two ring gaps and back-to-back varactors. Fabricated filter with (b) close-up view and (c) full view. The dimensions of the filter are labeled in (d) and (e).

in section V-A. When  $C_{Qez}$  is not included,  $TZ_4$  is not seen within 2 GHz frequency range. However, when  $C_{Qez} = 1.5$  pF is included,  $TZ_4$  appears around 1.9 GHz in Fig. 21(b), which agrees well with Fig. 19. The location of  $TZ_4$  appears independent of the BW tuning, which makes this TZ ideal for rejecting fixed spurious resonances or interferences.

Fig. 21(c) shows measured  $S_{21}$  when the filter is in the off-state:  $k_E \approx k_M$  and the two resonators are asynchronously tuned to 0.58 GHz and 1.15 GHz to improve isolation. More than 30 dB of off-state isolation is achieved up to 2 GHz. As

TABLE III  
SURFACE MOUNT LUMPED COMPONENTS

Type	#	Model	Value (pF)	Q @ 50 MHz
$C_{fo}$	64	Skyworks SMV1405	0.63-2.67	3200
$C_{BW}$	2	Skyworks SMV1405	0.63-2.67	3200
$C_{Qe}$	12	Infineon BB857H7902	0.55-6.6	1000
$C_{Qez}$	2	Johanson Techno. S-Series	1.5	5000

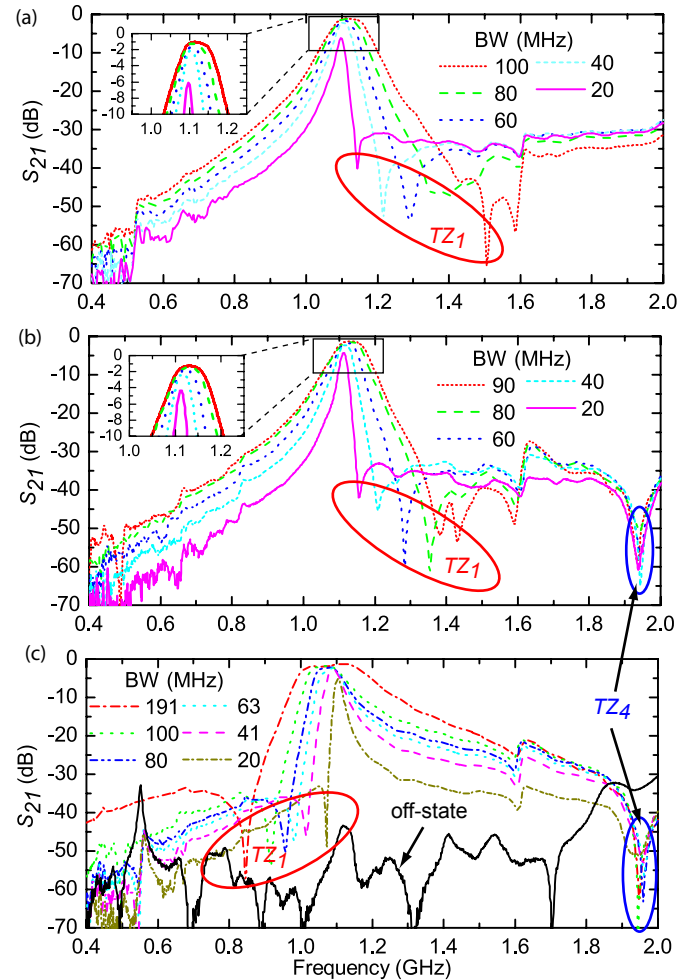


Fig. 21. (a) Measured  $S_{21}$  shows both BW and  $TZ_1$  decrease as  $C_{BW}$  increases. (b)  $TZ_4$  appears around 1.95 GHz when  $C_{Qez} = 1.5$  pF is added. (c) As  $C_{BW}$  increases further,  $TZ_1$  moves below the passband while BW increases. An off-state is also measured with the resonators asynchronously tuned.

$C_{BW}$  increases from the off-state,  $k_E$  becomes dominant and the BW increases again.  $TZ_1$  has moved below the passband and moves further from the passband as  $C_{BW}$  increases. Though a larger BW range is possible for this filter when  $k_E$  is dominant, the loss is also higher since more energy is flowing through the lossy  $C_{BW}$  varactor.

Fig. 22 shows the measured  $S_{21}$  and  $S_{11}$  for center frequency and BW tuning range. Typical examples of Butterworth and Chebyshev filter responses are shown. This figure can be compared to Fig. 17 where the tuning ranges are predicted from HFSS simulation. Both simulation and measured data shows a center frequency tuning range of 0.55–1.1 GHz. Table IV compares the simulation versus measured range of

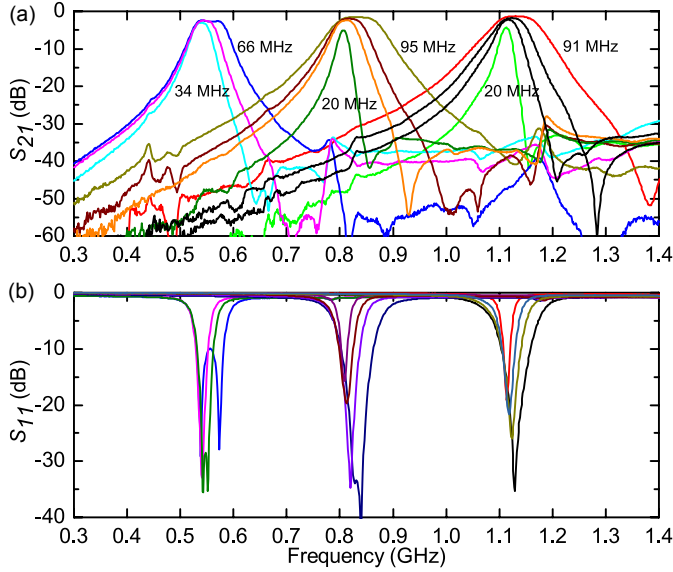


Fig. 22. Measured (a)  $S_{21}$  and (b)  $S_{11}$  showing both tunable center frequency and tunable BW.

BW. The measured and simulated BW ranges match closely. The measured FBW is 6.18–12% at 0.55 GHz, 2.38–11.3% at 0.84 GHz, and 1.77–8.05% at 1.1 GHz. For the measurement, a 10 dB minimum return loss and 20 MHz minimum BW criteria limits the range. Peak insertion loss of 1.28 dB at 1.13 GHz is measured and about 30 dB of out-of-band rejection is maintained up to 2 GHz. The extracted  $Q_u$  for the resonators is approximately 80 at 0.5 GHz and 200 at 1.1 GHz.

TABLE IV  
SIMULATION VERSUS MEASURED BW RANGE

Freq. (Ghz)	Simulation BW (MHz)	Measured BW (MHz)
1.1	30–87	20–91
0.84	14–91	20–95
0.55	37–60	34–66

For some tunable filter applications, maintaining a constant BW or constant FBW maybe desirable. This filter can achieve a constant BW anywhere from 34 MHz to 66 MHz and a larger BW range is possible with a reduced frequency tuning range such as 20 MHz to 90 MHz BW from 0.7 to 1.13 GHz. As examples, Fig. 23(a) shows 60 MHz 3-dB constant BW tuning with insertions loss between 1.9 dB and 2.3 dB and return loss better than 14 dB, while Fig. 23(b) shows 8% 3-dB FBW tuning with insertion loss between 1.28 dB and 1.7 dB and return loss better than 30 dB. More than 30 dB of out band rejection is maintained in both cases.

### C. Tunable TZ Four-Pole Filter

Fig. 24 shows filter  $M_4$  (Fig. 9(a) and Eqn. (15) from Section III-C modified to a tunable filter. Two MACOM MA46H120 varactors ( $Q$  of 3000 at 50 MHz) are soldered back to back on each resonator to tune the center frequency. The MACOM varactors have a capacitance range of 0.13–1.1 pF. Measured results in Fig. 25 shows the center frequency

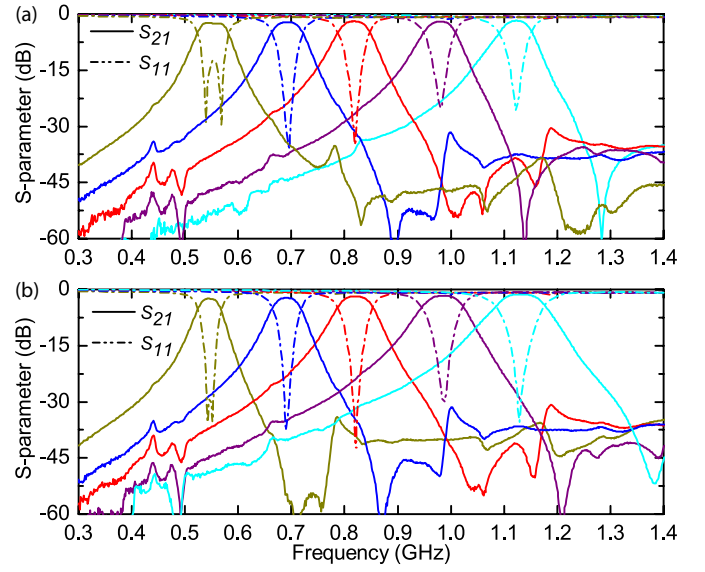


Fig. 23. Measured  $S_{21}$  and  $S_{11}$  for a (a) 60 MHz constant absolute 3-dB BW and (b) 8% constant 3-dB FBW.

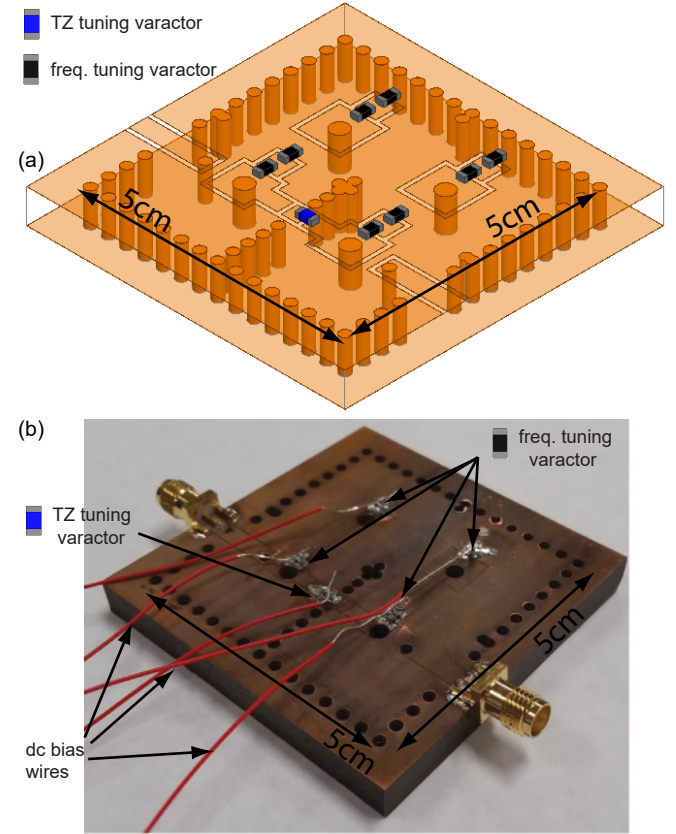


Fig. 24. (a) Designed and (b) fabricated four-pole filter with tunable center frequency and tunable TZs.

of the four-pole filter tunes from 2.24 GHz to 2.64 GHz with the peak pass band insertion loss ranging from 3.9 dB to 3.4 dB. The 3-dB FBW increases from 9% to 10.8% as the center frequency increases. The return loss of the filter is at least 10 dB through out the tuning range.

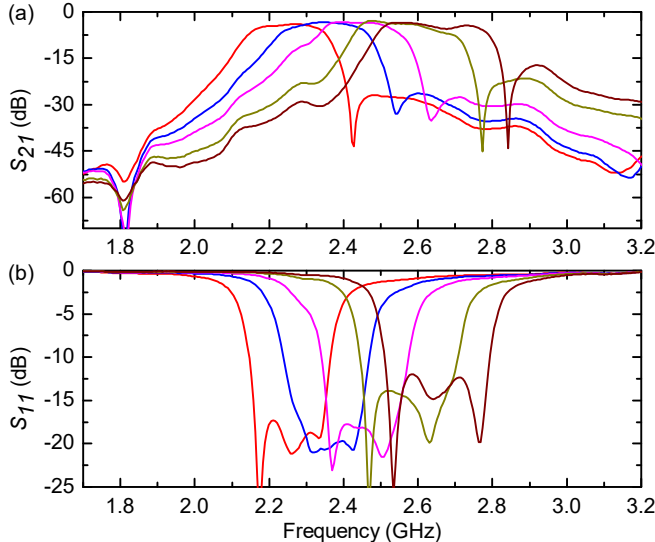


Fig. 25. Measured (a)  $S_{21}$  and (b)  $S_{11}$  of four-pole filter showing tunable center frequency.

Similar to the results in section III-C, three TZs are created. However in this case an additional MACOM MA46H120 varactor ( $C_{TZ}$ ) is used to tune the capacitive cross-coupling between resonator 1 and 4. Since the cross-coupling in filter  $M_4$  is strongly capacitive (section III-C), as  $C_{TZ}$  increases the magnitude of cross-coupling also increases and  $TZ_2$  and  $TZ_3$  move closer to the passband. Fig. 26 shows the simulated and measured results of the filter while the capacitive cross-coupling is tuned. Since electric coupling is dominant,  $TZ_1$  is below the passband and as the  $C_{TZ}$  increases,  $TZ_1$  frequency decreases.

## VI. CONCLUSION

This work presents a planar structure for realizing mixed electric and magnetic dispersive coupling in substrate-integrated coaxial-cavity filters. Surface mount components are easily integrated into the filter to allow for flexible control of the filter center frequency, bandwidth, and locations of the transmission zeros. Filter design methodologies based on a dispersive coupling structure are presented using lumped circuit models, coupling matrix, and full-wave simulations. In addition, the external coupling structure can add another TZ above the passband. Fabricated two-pole filters with one or two TZs and four-pole filters with three or four TZs validate the filter design. A frequency and BW tunable filter shows tuning range from 0.55 GHz to 1.1 GHz with a BW of 20–91 MHz at 1.1 GHz, 20–95 MHz at 0.84 GHz, and 34–66 MHz at 0.55 GHz. A four-pole filter with tunable center frequency and tunable transmission zeros is also demonstrated.

## REFERENCES

- [1] C. K. Richard Cameron and R. Mansour, *Microwave Filters for Communication Systems: Fundamentals, Design and Applications*. Hoboken, New Jersey: John Wiley and Sons, 2007.
- [2] K. Wu, D. Deslandes, and Y. Cassivi, "The substrate integrated circuits - a new concept for high-frequency electronics and optoelectronics," in *International Conference on Telecommunications in Modern Satellite, Cable and Broadcasting Service*, vol. 1, Oct 2003, pp. P-III-P-X vol.1.
- [3] K. Entesari, A. Saghati, V. Sekar, and M. Armendariz, "Tunable siw structures: Antennas, vcos, and filters," *IEEE Microwave Magazine*, vol. 16, no. 5, pp. 34–54, June 2015.
- [4] J.-S. Hong, *Microstrip Filters for RF/Microwave Applications*. New York: Wiley, 2011.
- [5] I. Hunter, *Theory and Design of microwave Filters*. London, United Kingdom: The Institution of Electrical Engineers, 2001.
- [6] J.-S. Zhan and J.-L. Wang, "A simple four-order cross-coupled filter with three transmission zeros," *Progress In Electromagnetics Research*, vol. 8, pp. 57–68, 2009.
- [7] S. Amari and J. Bornemann, "Using frequency-dependent coupling to generate finite attenuation poles in direct-coupled resonator bandpass filters," *IEEE Microwave and Guided Wave Letters*, vol. 9, no. 10, pp. 404–406, Oct 1999.
- [8] W. Shen, L.-S. Wu, X.-W. Sun, W.-Y. Yin, and J.-F. Mao, "Novel substrate integrated waveguide filters with mixed cross coupling (mcc)," *IEEE Microwave and Wireless Components Letters*, vol. 19, no. 11, pp. 701–703, Nov 2009.
- [9] K. Gong, W. Hong, Y. Zhang, P. Chen, and C. J. You, "Substrate integrated waveguide quasi-elliptic filters with controllable electric and magnetic mixed coupling," *IEEE Transactions on Microwave Theory and Techniques*, vol. 60, no. 10, pp. 3071–3078, Oct 2012.
- [10] E. Naglich, D. Peroulis, and W. Chappell, "Wide spurious free range positive-to-negative inter-resonator coupling structure for reconfigurable filters," in *IEEE MTT-S International Microwave Symposium Digest*, June 2013, pp. 1–4.
- [11] A. Anand and X. Liu, "Capacitively tuned electrical coupling for reconfigurable coaxial cavity bandstop filters," in *IEEE MTT-S International Microwave Symposium Digest*, May 2015, pp. 1–3.
- [12] A. Guyette, "Alternative architectures for narrowband varactor-tuned bandpass filters," in *European Microwave Integrated Circuits Conference*, Sept 2009, pp. 475–478.
- [13] P. Wong and I. Hunter, "Electronically reconfigurable microwave bandpass filter," *IEEE Transactions on Microwave Theory and Techniques*, vol. 57, no. 12, pp. 3070–3079, Dec 2009.
- [14] C. H. Kim and K. Chang, "Ring resonator bandpass filter with switchable bandwidth using stepped-impedance stubs," *IEEE Transactions on Microwave Theory and Techniques*, vol. 58, no. 12, pp. 3936–3944, Dec 2010.
- [15] Y.-C. Chiou and G. Rebeiz, "A tunable three-pole 1.5-2.2-ghz bandpass filter with bandwidth and transmission zero control," *IEEE Transactions on Microwave Theory and Techniques*, vol. 59, no. 11, pp. 2872–2878, Nov 2011.
- [16] H.-J. Tsai, N.-W. Chen, and S.-K. Jeng, "Center frequency and bandwidth controllable microstrip bandpass filter design using loop-shaped dual-mode resonator," *IEEE Transactions on Microwave Theory and Techniques*, vol. 61, no. 10, pp. 3590–3600, Oct 2013.

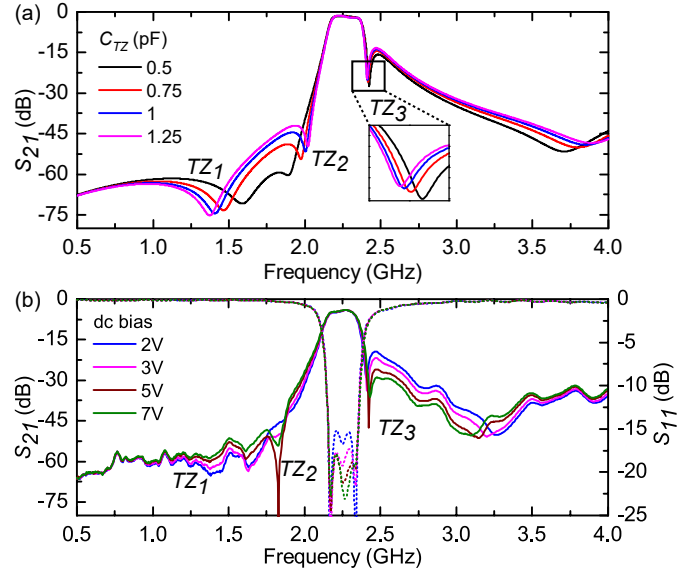
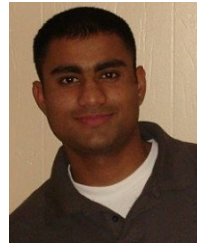


Fig. 26. (a) Simulated and (b) measured s-parameters of four-pole filter showing tunable TZs.

- [17] J.-R. Mao, W.-W. Choi, K.-W. Tam, W. Q. Che, and Q. Xue, "Tunable bandpass filter design based on external quality factor tuning and multiple mode resonators for wideband applications," *IEEE Transactions on Microwave Theory and Techniques*, vol. 61, no. 7, pp. 2574–2584, July 2013.
- [18] Y. Deng and K. Wu, "Compact bandpass filter with tunable center frequency and reconfigurable bandwidth," in *European Microwave Conference*, Oct 2013, pp. 1027–1030.
- [19] Y.-H. Cho and G. Rebeiz, "Two- and four-pole tunable 0.7-1.1-ghz bandpass-to-bandstop filters with bandwidth control," *IEEE Transactions on Microwave Theory and Techniques*, vol. 62, no. 3, pp. 457–463, March 2014.
- [20] C.-C. Cheng and G. Rebeiz, "High-q 4-6 ghz suspended stripline rf mems tunable filter with bandwidth control," *IEEE Transactions on Microwave Theory and Techniques*, vol. 59, no. 10, pp. 2469–2476, Oct 2011.
- [21] A. Anand and X. Liu, "Substrate-integrated coaxial-cavity filter with tunable center frequency and reconfigurable bandwidth," in *Wireless and Microwave Technology Conference (WAMICON), 2014 IEEE 15th Annual*, June 2014, pp. 1–4.
- [22] T. Yang, K. Ho, and G. Rebeiz, "Compact self-shielded 2–3 ghz high-q coaxial fixed and tunable filters," *IEEE Transactions on Microwave Theory and Techniques*, vol. 62, no. 12, pp. 3370–3379, Dec 2014.
- [23] S. Sirci, F. Gentili, J. D. Martinez, V. E. Boria, and R. Sorrentino, "Quasi-elliptic filter based on siw combline resonators using a coplanar line cross-coupling," in *2015 IEEE MTT-S International Microwave Symposium*, May 2015, pp. 1–4.
- [24] S. Sirci, M. . Sánchez-Soriano, J. D. Martinez, V. E. Boria, F. Gentili, W. Bschi, and R. Sorrentino, "Design and multiphysics analysis of direct and cross-coupled siw combline filters using electric and magnetic couplings," *IEEE Transactions on Microwave Theory and Techniques*, vol. 63, no. 12, pp. 4341–4354, Dec 2015.
- [25] R. J. Wenzel, "Exact design of wideband equal-ripple bandpass filters with non-adjacent resonator couplings," in *IEEE-MTT-S International Microwave Symposium*, June 1976, pp. 125–127.
- [26] L. Szydłowski, A. Lamecki, and M. Mrozowski, "Coupled-resonator waveguide filter in quadruplet topology with frequency-dependent coupling-a design based on coupling matrix," *IEEE Microwave and Wireless Components Letters*, vol. 22, no. 11, pp. 553–555, Nov 2012.
- [27] J. Martinez, M. Taroncher, and V. Boria, "Capacitively loaded resonator for compact substrate integrated waveguide filters," in *European Microwave Conference*, Sept 2010, pp. 192–195.
- [28] S. Sirci, J. Martinez, M. Taroncher, and V. Boria, "Varactor-loaded continuously tunable siw resonator for reconfigurable filter design," in *European Microwave Conference*, Oct 2011, pp. 436–439.
- [29] ———, "Analog tuning of compact varactor-loaded combline filters in substrate integrated waveguide," in *European Microwave Conference*, Oct 2012, pp. 257–260.
- [30] A. Anand, J. Small, M. S. Arif, M. Sinani, D. Peroulis, and X. Liu, "A novel high-qu octave-tunable resonator with lumped tuning elements," in *IEEE MTT-S International Microwave Symposium Digest*, June 2013, pp. 1–3.
- [31] A. Anand, Y. Liu, and X. Liu, "Substrate-integrated octave-tunable combline bandstop filter with surface mount varactors," in *Wireless Symposium (IWS), 2014 IEEE International*, March 2014, pp. 1–4.
- [32] A. Anand, J. Small, D. Peroulis, and X. Liu, "Theory and design of octave tunable filters with lumped tuning elements," *IEEE Transactions on Microwave Theory and Techniques*, vol. 61, no. 12, pp. 4353–4364, Dec 2013.
- [33] H. Wang and Q.-X. Chu, "Generation of transmission zero through electric and magnetic mixed coupling," in *International Conference on Microwave and Millimeter Wave Technology*, April 2007, pp. 1–3.
- [34] D. Swanson, "Narrow-band microwave filter design," *IEEE Microwave Magazine*, vol. 8, no. 5, pp. 105–114, Oct 2007.
- [35] D. Deslandes and K. Wu, "Analysis and design of current probe transition from grounded coplanar to substrate integrated rectangular waveguides," *IEEE Transactions on Microwave Theory and Techniques*, vol. 53, no. 8, pp. 2487–2494, Aug 2005.
- [36] R. Levy, "Filters with single transmission zeros at real or imaginary frequencies," *IEEE Transactions on Microwave Theory and Techniques*, vol. 24, no. 4, pp. 172–181, Apr 1976.
- [37] A. Atia and A. Williams, "Narrow-bandpass waveguide filters," *IEEE Transactions on Microwave Theory and Techniques*, vol. 20, no. 4, pp. 258–265, Apr 1972.
- [38] J. Thomas, "Cross-coupling in coaxial cavity filters - a tutorial overview," *IEEE Transactions on Microwave Theory and Techniques*, vol. 51, no. 4, pp. 1368–1376, Apr 2003.
- [39] X. Wang, G. Jang, B. Lee, and N. Park, "Compact quad-mode bandpass filter using modified coaxial cavity resonator with improved q -factor," *IEEE Transactions on Microwave Theory and Techniques*, vol. 63, no. 3, pp. 965–975, March 2015.
- [40] M. El-Tanani and G. Rebeiz, "A two-pole two-zero tunable filter with improved linearity," *IEEE Transactions on Microwave Theory and Techniques*, vol. 57, no. 4, pp. 830–839, April 2009.



**Aakash Anand** (S'12) received his B.S. and M.S. degrees in electrical engineering from University of California, Davis in 2009 and 2014. He is currently working towards his Ph.D. degree at University of California, Davis. His research interest is in RF and millimeter wave circuits including filters and tunable filters, RFICs and analog ICs, frequency synthesizers, and RF systems. He has previously worked for Intel Corporation, BAE Systems, and Keysight Technologies and is currently working for Nuvotonics.



**Dr. Xiaoguang "Leo" Liu** (S'07–M'10) received his B.S. degree from Zhejiang University, China in 2004 and his Ph.D. degree from Purdue University in 2010. He is currently an assistant professor in the Department of Electrical and Computer Engineering at the University of California, Davis. His research interests include radio RF-MEMS devices and other reconfigurable high frequency components, high frequency integrated circuits, and biomedical and industrial applications of high frequency communication and sensing systems.